PUMPING OF WATER WITH ROTATING ELECTRIC FIELDS AT THE NANOSCALE

Sergio De Luca[1], B.D.Todd[1], Jesper S. Hansen[2], Peter J. Daivis[3]

[1]Mathematics, Swinburne University of Technology, Melbourne Victoria 3122, Australia
[2]Department of Science, Systems and Models, Roskilde University, DK-4000, Roskilde, Denmark
[3]Department of Applied Physics, RMIT University, Melbourne, Victoria 3001, Australia

ABSTRACT

We present the first non-equilibrium molecular dynamics results for pumping of water at the nanoscale, utilizing a new, completely non intrusive approach. The flow production is sustained by means of a body force acting on the polar molecules in the form of an external, spatially uniform rotating electric field. The theoretical background relies upon the coupling of the spin angular momentum to linear streaming momentum, enhanced when the interaction of the permanent dipole moment of the molecules with the external field is significant. By further embedding the small fluid volume between two different planar surfaces, one hydrophobic and one hydrophilic, it is possible to generate unidirectional fluid flow. Concomitantly, by properly tuning the frequency and strength of the external field, moderate fluid operational temperatures can be maintained, thereby revealing some exciting and potentially useful applications in the field of nanotechnology.

INTRODUCTION

Manipulation and generation of fluid flow at the micro-nanoscale is usually achieved by micropumps exerting pressure on the fluid by means of moving solid boundaries, or by exerting forces directly onto the fluid, for instance by means of an external electric fields. Among the techniques belonging to the second category, electroosmotic micropumps constitutes a widespread and efficient methodology to drive flow, based on the draining effect of dissolved ions in liquids, subjected to an external dc field. We use a completely new method to pump fluid flow of polar molecules, that requires neither any form of intrusive mechanical device into the fluid, or any addition of solute carrier charges. The mechanism rests on the coupling of the spin angular momentum to linear translational motion of a highly confined polar fluid (water as one of the most important examples). We have shown that ignoring the coupling of spin angular momentum to linear translational motion of a highly confined fluid can lead to significant overestimation of the predicted flow rates using conventional Navier-Stokes treatments. By including spin-coupling into the extended Navier-Stokes equations, hydrodynamic prediction is seen to be very accurate down to length scales of a few atomic diameters [1]. We also demonstrate how this knowledge, coupled with our knowledge of the different behaviour of dipolar liquids when confined between hydrophobic and hydrophilic solid surfaces, can be used to pump molecular fluids such as water via non-intrusive application of a rotating electric field [2,3]. By both theoretical modelling and nonequilibrium molecular dynamics (NEMD) simulations of such a system we show that a steady uni-directional flow can be generated at microwave frequency ranges using external rotating electric fields[4].

METHODS

We performed NEMD simulations of N = 270 water molecules confined between two planar surfaces, distinguishable for the different crystal structure and surface charge characteristics. A schematic of the system is reported in Fig (1), which represents an asymmetric channel. From a mathematical point of view, the asymmetric channel reproduce the different velocity boundary conditions near the interfaces. The hydrophilic wall implements a BCC (body-centered-cubic) crystal structure, with the addition of small dipole charges (not visible) to enforce the no-slip velocity boundary condition at this interface. The hydrophobic wall particles are distributed in conformity with the FCC (face-centered-structure) crystal structure, such that the density is larger than the hydrophilic wall. Further details on the construction of the channel surfaces are given in [4]. We emphasize at this point that the use of the asymmetric channel is a necessary condition for having a net flow production along the channel. Fluid volumes confined between two equal hydrophobic or two equal hydrophilic walls result in a zero net flow, as we will see in the next section.

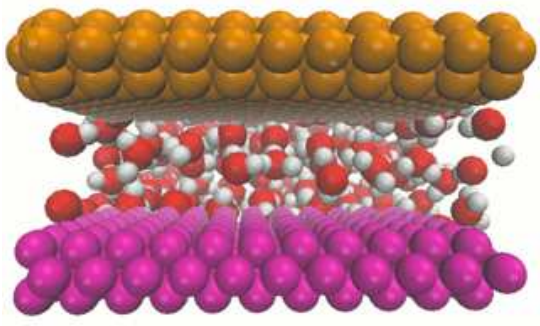

Fig. 1. System composed of two planar walls confining water molecules. The yellow wall represents a hydrophobic surface while the purple wall models the hydrophilic side.

Liquid water is modeled with the SPC/E pair potential [5], with partial charges q_H = 0.4238 e and q_O = -0.8476 e for hydrogen and oxygen, respectively (e = 1.6×10^{-19} C is the fundamental unit of charge). Bonds and angles are constrained with the SHAKE algorithm [6]. Molecule interactions are modeled by means of the Lennard-Jones (LJ) pair potential, with the addition of the Coulomb term for the charged particles, which reads

$$\Phi = \sum_i \sum_{j>i} 4\varepsilon \left[\left(\frac{\sigma}{r_{ij}} \right)^{12} - \left(\frac{\sigma}{r_{ij}} \right)^{6} \right] + \sum_i \sum_{j>i} \frac{q_i q_j}{r_{ij}} \qquad (1)$$

with the energy scale parameter ε = 0.65 Kj mol^{-1} and the length scale parameter σ = 0.32 nm. The sum extends over the total number of the molecules, noting that the indices i and j do not belong to the same molecule. The r_{ij} term represents the distance between the particles, i.e. the sites of different water molecules and between water and wall particles. The Coulomb term, representative of the long range electrostatic interactions, is incorporated in the Wolf algorithm [7]. The simulation box sides are L_x = 1.9 nm, L_y = 4.5 nm and L_z = 1.9 nm, and the vertical separation between the two plates is 2.25 nm (*y*-direction in Fig. (1)). This configuration yields the density of water ρ = 998 Kg/m^3. The *x* axis corresponds to the flow direction, i.e. from the right to the left side of Fig. (1) and the *z*-axis is perpendicular to the other two. Both the *x* and *z* axes are treated as periodic. To avoid expensive and unnecessary force computations, the LJ interaction potential is truncated at the distance *r* = 1 nm.

The external rotating electric field, which acts on the sites of the water molecule, is spatially uniform and time dependent, and can be represented with the vector E = [cos(ωt), sin(ωt), 0], where ω is the angular frequency and t is the time. The resulting electric field is polarized along the plane generated from the direction perpendicular to the two surfaces (*x*-axis, see Fig (1)) and parallel to the two plates, from the left to the right of the same figure (*x*-direction). The action of the electric field results in the torque exerted on the water permanent dipoles

$$\vec{\tau} = \sum_i (\vec{r}_i - \vec{r}_{CM}) \times q_i \vec{E}_i \qquad (2)$$

with the sum ranging over the three sites of the SPC/E water, $\vec{r}_i$ and $\vec{r}_{CM}$ vector positions of the site *i* and the center of mass of the water molecule, q_i and $\vec{E}_i$ represent the charge attached to the site *i* and the electric field acting on the particle positions. The torque injected into fluid constrains the dipole moments to align with the field. This alignment tendency competes with the disordering effect of the thermal energy but, with a proper choice of the amplitude and frequency of the field, generates an average rotation of the dipoles along the *z*-direction, which in turn gives rise to a net flow rate production (in the asymmetric channel).

The leap-frog scheme was used to integrate the Newtonian equations of motion for the fluid and wall particles [8], with the time step Δt = 1.6 fs which yields a good stability of the integrator. Full details on the integrator implementation, in conjunction with the insertion of the external body force term in the algorithm are given in [4]. The work supplied by the external field on the fluid results in a thermal energy increase, due to the enhanced friction between molecules. The heating produced is removed with the Nosé-Hoover thermostat applied only to the wall particles [9-11]. To implement this technique, the wall atoms are forced to oscillate around their equilibrium positions, subjected to an elastic force whose strength is tuned to optimize the thermostat efficiency, maintaining at the same time the proper stability of the crystal wall structure. This approach has the merit to leave the rotational degree of freedom of the water molecules unaltered [12-15].

At the beginning of the simulation, the system is allowed to equilibrate and typically relaxes in a configuration of minimum potential energy approximately after 500 ps. Then the field is turned on and after 5-6 ns achieves steady state, which means that all the physical properties of interest, like velocity and temperature, attain approximately constant values. Averages are accumulated in the next 7 ns implementing standard binning techniques [16], with 200 bins of width 0.02 nm. The aforementioned properties are plotted against the distance between the two surfaces (*y*-direction) and are evaluated from their microscopic definition. The streaming velocity profile has been computed by means of

$$v_x(y) = \frac{\left\langle \sum_i m_i v_{x,i} \delta(y_i - y) \right\rangle}{\left\langle \sum_i m_i \delta(y_i - y) \right\rangle} \qquad (3)$$

i.e. the momentum flux density

$$J_x(\vec{r}, t) = \sum_i m_i v_{x,i} \delta(\vec{r} - \vec{r}_i) \qquad (4)$$

is divided by the mass density

$$\rho = \sum_i m_i \delta(\vec{r} - \vec{r}_i) \qquad (5)$$

where *i* ranges over the molecule *i*, m_i is the mass of a water molecule, $v_{x,i}$ represents the velocity component of the *i*-th molecule in the direction parallel to the surfaces and $\vec{r}_i$ is the center of mass location of molecule *i*. The angle brackets in (3) stand for time averages, to be taken at the end of the simulation run. The response of the fluid system to the external field is further investigated averaging the molecular temperature profile (computed with the aforementioned binning technique)

$$T_{mol} = \frac{1}{3 K_B N} \sum_i m_i \vec{c}^{\,2}_{i,cm} \qquad (6)$$

with *N* the total number of water molecules, k_B the Boltzmann constant and $\vec{c}^{\,2}{}_{i,cm}$ the square of the thermal velocity of the *i*-th water molecule center of mass.

RESULTS

We plot in Fig. 2 the streaming velocity profile, computed from Eq. (3), for the asymmetric channel depicted in Fig (1). The picture overlaps ten independent simulations, with the electric field amplitude kept fixed at 1.8 V/nm whereas the frequency ranges from 10 to 100 GHz, in steps of 10 GHz. The profile with the smallest slope, indicated in the picture with the *x* symbol, corresponds to the frequency of 10 GHz. Increasing the frequency from 20 GHz to 90 GHz, (see profiles drawn with solid lines in Fig. (2)), coincides with a monotonically increasing absolute value of the slope, which in turn means a larger value of the absolute streaming velocity next to the hydrophobic side. The case with the highest frequency, 100 GHz, depicted in Fig (2) with the asterisk symbol, gives an absolute streaming velocity adjacent to the hydrophobic side (right side of the picture) of approximately 100 m/s. Note that for frequencies larger than 120 GHz, a value which corresponds to the inverse of the dipolar relaxation time of water, the trend reverses and the absolute velocities decrease as the frequency increases (not shown)

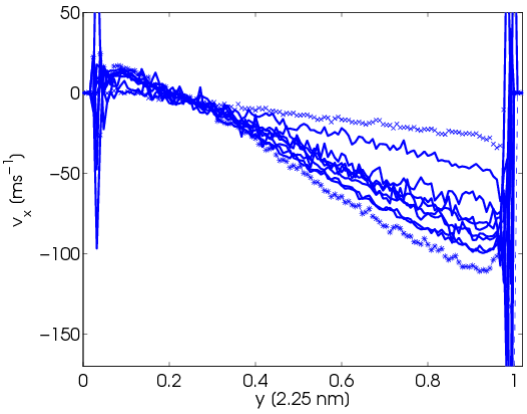

Fig. 2. Streaming velocity profile of water for the asymmetric channel. The hydrophilic wall is located on the left side and the hydrophobic wall on the right side.

To clarify the dependence of the streaming velocity on the frequency of the external field, we plot in Fig. (3) the maximum (absolute) values of the velocities adjacent to the hydrophobic side, as plotted in Fig. (2). For the field frequency 10 GHz up to the final value 100 GHz, the absolute value of the streaming velocity increases. Moreover, we see that the trend is nonlinear and that at the highest frequencies the velocity begins to saturate at values close to $v_x = 100$ m/s. This saturation point also depends on the amplitude of the electric field. In Fig. (4) we report the maximum (absolute) streaming velocity values, next to the hydrophobic wall, for the case of fixed field frequency and varying amplitude. We investigate the amplitude range from 1 V/nm up to 10 V/nm, at the same time keeping the frequency fixed at 20 GHz. Again, we see an increase of the absolute streaming velocity as the amplitude intensifies from the strength value 0.8 V/nm. For amplitude values of the order of 3-4 V/nm the streaming velocities saturate again

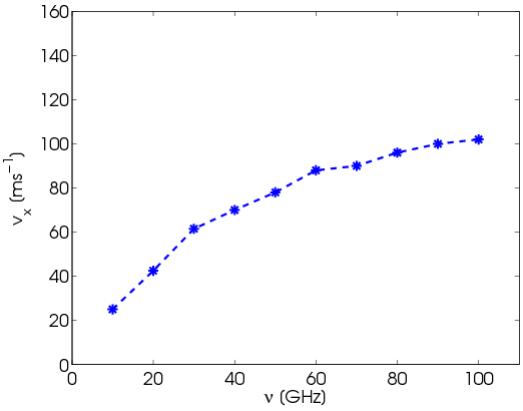

Fig. (3). Maximum (absolute) streaming velocity of water for the asymmetric channel. The amplitude is fixed at 1.8 V/nm.

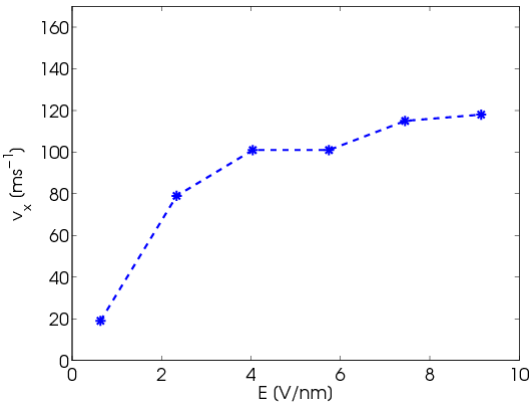

Fig. 4. Maximum (absolute) streaming velocity of water for the asymmetric channel. The field frequency is fixed at 20 GHz.

towards the approximate value 110 m/s. The explanation of this tendency relies on Eq. (2), in which a larger amplitude of the electric field results in an increase of the torque injected into the fluid. Again, the velocities begin to saturate around 3 V/nm, stabilizing approximately at 100 m/s.

The work performed by the external electric field on the fluid volume is partly converted in translational kinetic energy (due to the coupling between the spin angular momentum to linear streaming momentum momentum) and partly is dissipated in internal energy. In Fig. (5) we show the temperature profiles for the same fluid system and external field parameters employed for the results of Fig. (2). The lowest temperature, depicted with the cross symbol, relates to the lowest frequency used, 10 GHz. Gradually increasing the frequency from 10 GHz to 90 GHz, yields a corresponding monotonic increase of the temperature. As the frequency of the field increases, the friction between dipoles is enhanced, due to the faster alignment of the dipole moments. The frequency of 100 GHz, the largest used in this work, corresponds the maximum heating of the fluid system (the top profile).

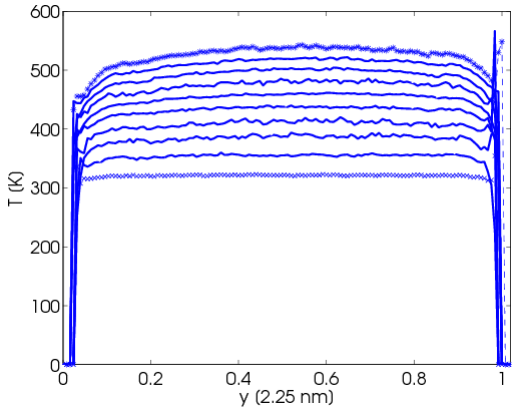

Fig. 5. Temperature profile of water for the asymmetric channel, corresponding to results reported in Fig. 2.

In Fig. (6) we plot the velocity profile with the field 1.8 V/nm and frequency 20 GHz for the symmetric channel. In this case, both surfaces are modelled with equal hydrophilic surfaces. The net flow rate production, i.e. the integrated area under the curve with respect the y-coordinate, is zero, since the two portion of area situated in the two halves of the channel are equal in magnitude but opposite in sign.

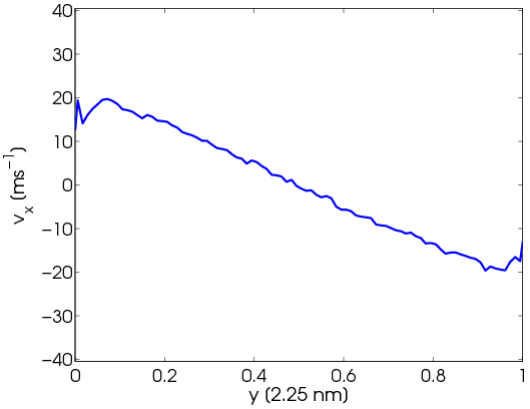

Fig. 6. Streaming velocity profile of water for the symmetric system. Amplitude and frequency are 1.8 V/nm and 20 GHz.

Finally, we compare our molecular dynamics results with the extended Navier-Stokes equations (ENS), which take into consideration the coupling of the spin angular momentum to the linear momentum [17-19]. The equations read:

$$\rho \frac{\partial v_x}{\partial t} = \rho F_e + (\eta_0 + \eta_r)\frac{\partial^2 v_x}{\partial y^2} - 2\eta_r \frac{\partial \Omega_z}{\partial y} \quad (7)$$

$$\rho I \frac{\partial \Omega_z}{\partial t} = \rho \Gamma_z + 2\eta_r \left(\frac{\partial v_x}{\partial y} - 2\Omega_z\right) + \varsigma \frac{\partial^2 \Omega_z}{\partial y^2} \quad (8)$$

We consider the asymmetric channel, with the amplitude set at 1.8 V/nm and the frequency at 20 GHz and we solve only Eq. (7), with respect to the streaming velocity v_x. Details on the streaming angular velocity solution Ω_z are given in [4]. The velocity boundary conditions, i.e. the streaming velocity v_x next to the two surfaces necessary to solve the second order partial differential equations, are 2.7 m/s for the hydrophilic wall and -45 m/s for the hydrophobic surface. F_e is the external force, set to zero as the electric field is the only external force acting on the system. The quantities Γ_z , η_0 η_r and ς represent the torque per unit mass injected into the system, the shear, vortex and spin viscosity, respectively. Note that the electric field enters the ENS by means of the torque term, as can be seen in Eq. (2). Specific considerations and technicalities are required for the selection of proper values for the torque term and for the fluid transport properties listed, detailed in [4] and references therein. As can be seen in Fig. (7) the agreement between the ENS numerical solutions and the NEMD profile result is excellent.

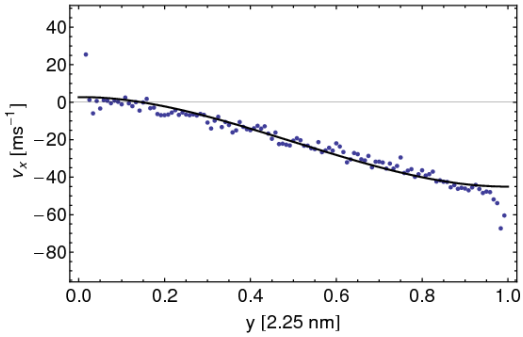

Fig. 7. NEMD streaming velocity profile of water (points) and numerical solution of the ENS (solid line) for the asymmetric channe.

CONCLUSIONS

We have demonstrated via nonequilibrium molecular dynamics simulations that a significant water flow production is attainable at the nanoscale, only exploiting the coupling between the spin angular momentum and the linear translational momentum. Furthermore, we showed that if the external field frequencies and amplitudes are properly tuned, then the temperature of the fluid can be maintained at reasonable low values. Finally, a good agreement between the extended Navier-Stokes equations and the NEMD results has been found. The non-intrusive characteristic of this water pumping method renders it attractive to the experimentalist, and may open the road for useful applications in the field of nanofluidics.

ACKNOWLEDGMENT

Computation utilized the Swinburne Supercomputer Centre, the Victorian Partnership for Advanced Computing HPC Facility and Support Services and an award under the Merit Allocation Scheme on the NCI National Facility at the Australian National University.

REFERENCES

[1] J. S. Hansen, J. C. Dyre, P. J. Daivis, B. D. Todd, H. Bruus, Nanoflow hydrodynamics, Phys. Rev. E, 84, 036311, 2011.

[2] J. D. Bonthuis, D. Horinek, L. Bocquet, R. R. Netz, Electrohydraulic power conversion in planar nanochannels, Phys. Rev. Lett., 103, 144503, 2009.

[3] J. S. Hansen, H. Bruus, B. D. Todd, P. J. Daivis, Rotational and spin viscosities of water: Application to nanofluidic, J. Chem. Phys.**,** 133, 144906, 2010.

[4] S. De Luca, B. D. Todd, J. S. Hansen, P. J. Daivis, Electropumping of water with rotating electric fields, J. Chem. Phys.**,** 138, 154712, 2013.

[5] H. J. C. Berendsen, J. R. Grigera, T. P. Straatsma, The missing term in effective pair potentials, J. Phys. Chem., 91, 6269, 1987.

[6] G. Ciccotti, M. Ferrario, J. P. Ryckaert, Molecular dynamics of rigid systems in cartesian coordinates: a general formulation, Mol. Phys. , 47, 1253, 1982.

[7] D. Wolf, P. Keblinski, S. R. Phillpot, J. Eggebrecht, Exact method for the simulation of the Coulombic systems by spherically truncated, pairwise r^{-1} summation, J. Chem. Phys. , 110, 8254, 1999.

[8] D. Rapaport, *The Art of Molecular Dynamics Simulation*, 2nd ed., Cambridge University Press, New York, 2004.

[9] S. Nosé, A unified formulation of the constant temperature molecular dynamics methods, J. Chem. Phys., 81, 511, 1984.

[10] S. Nosé, A molecular dynamics method for simulations in the canonical ensemble, Mol. Phys., 52, 255, 1984.

[11] W. G. Hoover, G. Canonical dynamics: Equilibrium phase-space distributions, Phys. Rev. A, 31, 1695, 1985.

[12] S. Bernardi, B. D. Todd, D. J. Searles, Thermostating highly confined fluids, J. Chem. Phys., 132, 244706, 2010.

[13] K. P. Travis, P. J. Daivis, D. J. Evans, Computer-simulation algorithms for molecules undergoing planar couette-flow - A nonequilibrium molecular-dynamics study, J. Chem. Phys., 103, 1109, 1995.

[14] K. P. Travis, P. J. Daivis, D. J. Evans, Thermostats for molecular fluids undergoing shear flow: Application to liquid chlorine, J. Chem. Phys., 103, 10638, 1995.

[15] K. P. Travis, P. J. Daivis, D. J. Evans, Erratum: Thermostats for molecular fluids undergoing shear flow: Application to liquid chlorine, J. Chem. Phys., 105, 3893, 1996.

[16] M. P. Allen, D. J. Tildesley, *Computer Simulation of Liquids*, Clarendon Press, Oxford., 1987.

[17] D. J. Evans, W. B. Streett, Transport properties of homonuclear diatomics II. Dense fluids, Mol. Phys., 36, 161, 1978.

[18] S. R. de Groot, P. Mazur, *Non-Equilibrium Thermodynamics*, Dover, Mineola, 1984.

[19] D. W. Condiff, J. S. Dahler, Fluid mechanical aspects of antisymmetric stress, Phys. Fluids, 7, 842, 1964.